



Evaluation of the corrosion resistance of an additive manufacturing steel using electrochemical techniques

Evaluación de la resistencia a la corrosión de un acero fabricado por manufactura aditiva mediante técnicas electroquímicas

Dayi Gilberto Agredo-Diaz ^{1a}, Arturo Barba-Pingarrón ^{2a}, Nicolas Ortiz-Godoy ^{1b}, Jesús Rafael González-Parra ^{2b}, Jhon Jairo Olaya-Florez ^{1c}, José Javier Cervantes-Cabello ^{2c}, Cesar Armando Ortiz-Otalora ³

¹ Facultad de Ingeniería, Departamento de Ingeniería Mecánica y Mecatrónica, Universidad Nacional de Colombia, Bogotá, Colombia. Orcid: ^a 0000-0003-2830-3022, ^b 0000-0003-4468-4603. Emails: ^a dgagredod@unal.edu.co, ^b nortizg@unal.edu.co, ^c jjolayaf@unal.edu.co

² Centro de Ingeniería de Superficies y Acabados-CENISA, Facultad de Ingeniería, División de Ingeniería Mecánica e Industrial, Universidad Nacional Autónoma de México, México. Orcid: ^a 0000-0001-7285-9429, ^b 0000-0002-6337-2931, ^c 0000-0001-6935-9300. Emails: ^a arbapin5@gmail.com, ^b rafael.parra@yandex.com, ^c cercab2@yahoo.com

³ Grupo de Investigación de Superficies Electroquímica y Corrosión-GSEC, Facultad de Ciencias, Escuela de Física, Universidad Pedagógica y Tecnológica de Colombia, Colombia. Orcid: 0000-0003-4943-3707. Email: cesar.ortiz@uptc.edu.co

Received: 20 May 2020. Accepted: 10 July 2020. Final version: 21 August 2020.

Abstract

Additive metal manufacturing has undergone a revolution in recent years, being able to be incorporated in several industries such as aeronautics, automotive and even in medicine, allowing the manufacture of complex parts with fewer steps in the process, which translates in material savings and cost reduction. In this work, the corrosion of low carbon steel obtained by depositing consecutive layers is carried out, using electrochemical impedance spectroscopy and electrochemical noise immersed in a 0.1 M NaCl solution, establishing a comparison between the metal of contribution and deposited material. The layers of the material are characterized microstructurally and mechanically using scanning electron microscopy and Vickers microhardness. Overall, the results show a good response of the material to the action of the electrolyte after the immersion time, on the other hand, the microstructural results allow identifying the formation of 3 zones due to the cooling of the material. The microhardness of the steel does not show great changes between the zones, however, there is a slight increase in the intermediate zone due to the reduction in grain size. These studies allow researchers to know the behavior of these materials in applications that require contact with corrosive solutions of this nature.

Keywords: additive manufacturing; electrochemical impedance; electrochemical noise; low carbon steel; scanning electron microscopy.

ISSN Printed: 1657 - 4583, ISSN Online: 2145 - 8456, CC BY-ND 4.0 

How to cite: D. G. Agredo-Diaz, A. Barba-Pingarrón, N. Ortiz-Godoy, J. R. González-Parra, J. J. Olaya-Florez, J. J. Cervantes-Cabello, C. A. Ortiz-Otalora, "Evaluation of the corrosion resistance of an additive manufacturing steel using electrochemical techniques," *Rev. UIS Ing.*, vol. 19, no. 4, pp. 213-222, 2020, doi: <https://doi.org/10.18273/revuin.v19n4-2020018>

Resumen

La manufactura aditiva de metales ha sufrido una revolución en los últimos años, pudiéndose incorporar en diversas industrias como la aeronáutica, automotriz e incluso en la medicina, permitiendo la fabricación de partes complejas con un menor número de pasos en el proceso, lo que se traduce en ahorro de material y reducción de costos. En este artículo se realiza el monitoreo del estado de corrosión de un acero de bajo carbono obtenido mediante la deposición de capas consecutivas, evaluándose a través de la técnica de impedancia electroquímica y ruido electroquímico, inmerso en una solución 0.1 M de NaCl, estableciendo una comparativa entre el metal de aporte y el material depositado. Las capas del material son caracterizadas microestructural y mecánicamente mediante microscopía electrónica de barrido y microdureza Vickers. De forma global, los resultados muestran una buena respuesta del material ante la acción del electrolito transcurrido el tiempo de inmersión, Por otro lado, los resultados microestructurales permiten identificar la formación de 3 zonas debido al enfriamiento en gradiente del material. La microdureza del acero no muestra grandes cambios entre las zonas, sin embargo, hay un ligero aumento en la zona intermedia debido a la reducción en el tamaño del grano. Estos estudios permiten a investigadores conocer el comportamiento de estos materiales en aplicaciones que demanden el contacto con soluciones corrosivas de esta naturaleza.

Palabras clave: acero de bajo carbono; impedancia electroquímica; manufactura aditiva; microscopía electrónica de barrido; ruido electroquímico.

1. Introduction

Additive manufacturing (**AM**) is a process in which a part or machine element is constructed from a three-dimensional model with the help of CAD-CAM software, by adding successive layers. [1-6]. Although these technologies are constantly evolving [7], there is still a limited state of the art on the effects that these materials can have under working conditions, especially corrosion. Authors such as Cervantes et al. [2], evaluated the mechanical performance of steels produced by additive manufacturing, Agredo et al. [8] analyzed the performance of these steels coated by electroless nickel plating in saline solutions, using electrochemical techniques. Zhang et al. [9] studied the mechanical and microstructural properties of stainless steel, finding significant variations of properties depending on the layers. Researchers like Liu et al. [10] evaluated the behavior of additively manufactured high-speed steel underwear and corrosion conditions.

It is important to know the performance of these steels subjected to severe environmental conditions, especially when they are in the presence of corrosive media such as industrial environments. For this reason, one of the main tools used is electrochemical techniques, which allow us to study the performance and predict what effects the materials may have when faced with the action of an electrolyte. Electrochemical impedance spectroscopy (**EIS**) is a technique that allows the study of the corrosion behavior of metallic materials. It is based on the application of a potential signal with magnitudes of the order of mV to the working electrode, a frequency scan is performed to obtain characteristic current values of the electrochemical behavior of the material under the

established conditions. The impedance results obtained can be represented in terms of a real and imaginary component (Nyquist diagram), an impedance modulus and a phase angle (Bode diagram). These diagrams can be associated with electrical circuits that represent the electrochemical processes occurring in the system [11-16].

Another newer and little-used technique is Electrochemical Noise (**EN**), which provides a detailed study of potential and current signal variations when the metal is in a corrosive medium. Malo and Uruchurtu [17], define noise as stochastic oscillations of potential and current. This allows to obtain information of the corrosion kinetics and to identify the corrosion mechanisms, through the interpretation by several methods, one of the most used is the time series, whose behavior allows to determine the types of corrosion that are appearing in the material. Another of the most implemented methods is the statistical one, where one of the most significant parameters is the standard deviation, for example, the decrease of the standard deviation of the potential is associated with the formation of a protective layer of oxides so it increases the resistance to corrosion [18-28].

An important measure in electrochemical noise is the resistance to noise R_n , which is related as the ratio of the standard deviation of the potential between the standard deviation of the current [29], this parameter allows tracking the corrosion as a function of time and relate it directly to the corrosion resistance of materials, equation 1 shows this correlation.

$$R_n = \frac{\sigma_E}{\sigma_I} \quad (1)$$

A second measure to identify the type of corrosion is the location index (LI), Xia et al. [30] defined LI as the ratio of the standard deviation of the current to the RMS current, equation 2 shows the above.

$$LI = \frac{\sigma_I}{I_{rms}} \quad (2)$$

This research studies the behavior of low carbon steel manufactured by additive manufacturing when faced with the action of a 0.1 M NaCl solution. The behavior of the filler metal is evaluated (ER70S-6 solid micro-wire, AWS A5.18/A5.18M standard). EIS and EN techniques are used to track the state of corrosion and monitor the system from 0 hours to 1320 hours of immersion.

2. Materials and methods

The steel manufactured by AM was obtained from a MIG-Router CNC machine at the Facultad de Ingeniería-Universidad Nacional Autónoma de México. For this purpose, a solid filament is used, designated AWS ER70S-6, which is kept at a distance between the torch and the surface of 8 mm, in addition to the following parameters: a current of 80 A, a voltage of 35 V with an argon flow of 0.4247 m³/h, an electrode advance speed of 15 m/min; This process is done by superimposing 5 layers of material leaving a solidification time of 60 s between every 2 layers, these variables are considered optimal, to generate material with an adequate combination of mechanical properties, according to studies carried out by Cervantes et al. [2]. Figure 1 shows an outline of the process.

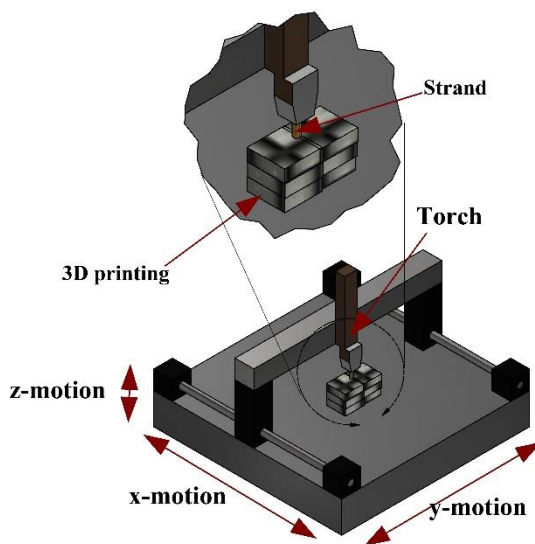


Figure 1. General scheme of the additive manufacturing process.

The elemental composition of the materials was obtained by atomic emission spectroscopy. The microstructural characterization of the filler material (strand) and the additive manufacturing steel was carried out by scanning electron microscopy (SEM) in a Phillips XL-20 electron microscope at HV=20 kV, WD=8.3 mm, and complemented by optical microscopy, the areas formed in the material after the printing process are characterized. The metallographic preparation was done by conventional polishing techniques implementing the ASTM E3 standard [31], the development of the microstructure was executed by Nital immersion at 2%.

The hardness of the layers was evaluated using a digital microdurometer model HVS-1000, with a load of 100 g-10 s, with a resolution of 0.1 HV. This characterization is carried out by taking measurements every 500 μm.

A Gill AC potentiostat controlled by the Sequencer software was used for electrochemical characterization. A 0.1 M de NaCl electrolyte was used and evaluated as a function of immersion time, using electrochemical impedance spectroscopy (EIS) and electrochemical noise (ENM) techniques, these were performed in a three-electrode electrochemical cell, composed by an SCE electrode as a reference, a graphite sheet as counter electrode and the material as working electrode, making a frequency sweep from 10⁴ to 10⁻¹ Hz, acquiring 10 points/decade, a sine wave with an amplitude of 10 mV was used as a perturbation. In electrochemical noise, time series of 1024 points every 0.5 s were obtained. Corrosion control was performed at 0, 240, 504, 1080 and 1320 h of immersion.

3. Results and discussion

3.1. Elemental composition and microstructure

The elemental composition of the strand is shown in table 1. Table 2 shows the elemental composition of the material produced by AM, which is the product of three random measurements on the sample.

Table 1. Elemental composition of the strand. % in weight

Fe	C	Mn	Si	Cu	Ni	Mo	Cr
Bal.	0.06-0.15	1.4-1.85	0.8-1.15	max-0.5	max-0.15	max-0.15	max-0.15

Source: [32].

Table 2. Elemental composition of additive manufacturing steel. % in weight

Fe	97.591
C	0.084
Mn	1.401
Si	0.808
Cu	0.052
Ni	0.013
Mo	0.015
Cr	0.012

This composition does not show significant variation as supplied by the strand manufacturer [32] and is within the range of AWS A5.18/A5.18M, these materials are classified as low carbon steels with high Mn content.

This composition does not show significant variation as supplied by the strand manufacturer [32] and is within the range of AWS A5.18/A5.18M, these materials are classified as low carbon steels with high Mn content.

Figure 2a shows the cross-section of the strand, here the high degree of plastic deformation in its microstructure is evident, which is the product of the wire drawing process applied to obtain this material. In figure 2b, a zoom in is observed. This allows to identify in more detail the orientation of the microstructure, which is oriented in the longitudinal direction (in the direction of the deformation process).

The microstructural study of the printed material shows the identification of 3 important areas. Figures 3 to 5 show: a first zone composed of the first two layers, an intermediate zone composed of layers 3 and 4, and an upper zone composed of the last layer, each with significant microstructural changes, each layer has an average thickness of 3000 μm .

Figure 3a shows the microstructure by optical microscopy of zone 1, the light areas correspond to ferrite and the dark areas to pearlite. In these two first layers, when the material is deposited on the support base it undergoes a process of rapid solidification, which favours a dendritic type growth, which is observed in figure 3b (SEM image). It is important to note that inclusions may occur in the deposited material (first two layers, figure 3b, circles in red), however, this is typical of the manufacturing process and is studied in detail by Cervantes et al. in [2], these defects do not exceed 5% of the material by volume.

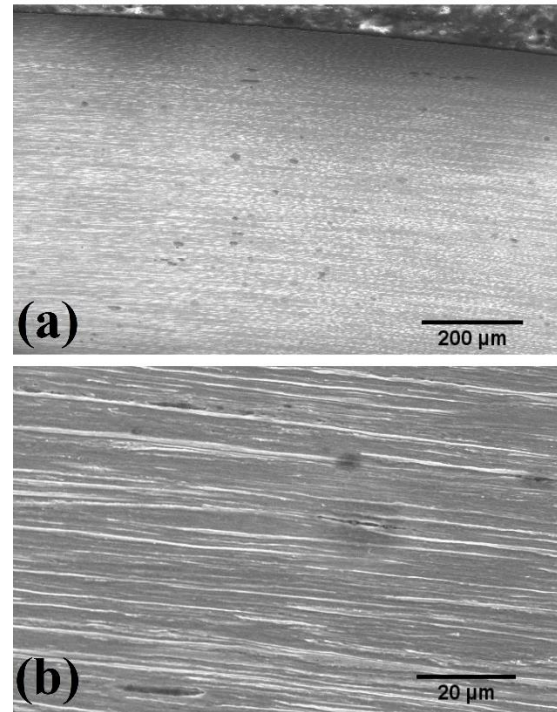


Figure 2. (a) SEM images with secondary electrons of the strand. (b) Zoom in on one of the strand areas.

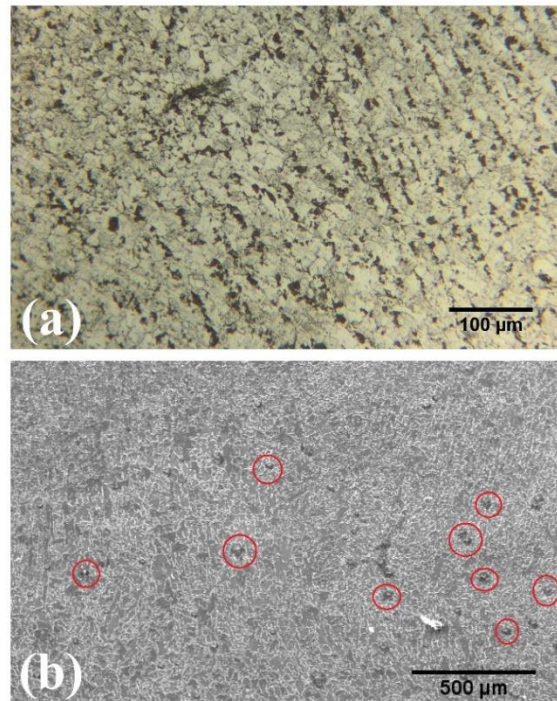


Figure 3. Zone 1 of steel produced by AM. (a) Optical microscopy image, (b) Scanning electron microscopy image with secondary electrons.

Zone 2, or intermediate zone, composed of the following two layers of material, shows a microstructure of ferrite and pearlite (Figure 4a) [2], [33]. In this zone a more homogeneous structure is evident with respect to zone 1, this homogeneity is associated to the fact that there are no thermal shocks, which generates a greater stability of the temperature obtaining a better distribution of the phases present, in figure 4b it can be observed at global level what was mentioned before. A zoom is made, which is shown in figure 4c, here it is possible to identify in more detail the phases present in the matter, for this case, the darkest area shows the ferrite phase, while the lightest area shows the pearlite phase.

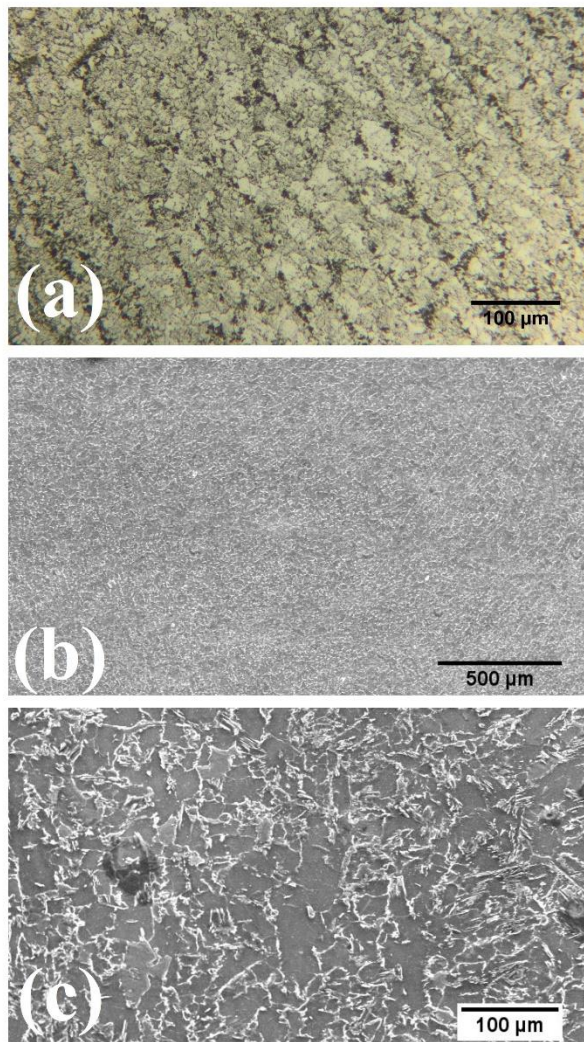


Figure 4. Zone 2 of steel produced by AM. (a) Optical microscopy image, (b) Scanning electron microscopy image with secondary electrons, (c) Amplification of the area.

The zone 3, or upper zone of the steel, composed of the last layer is shown in figure 5. Figure 5a shows the right lateral zone of the layer, where the orientation of the grains is observed, this tendency is generated by the high solidification speed in the material, in figure 5b and 5c the left lateral and central zone of the layer is shown, again the formation of a dendritic type structure predominates [34], condition that is linked to the solidification process [33], this high solidification speed is linked to the contact that the material has with the environment, which favors a heat transfer by convection. These results are consistent with those reported in [2].

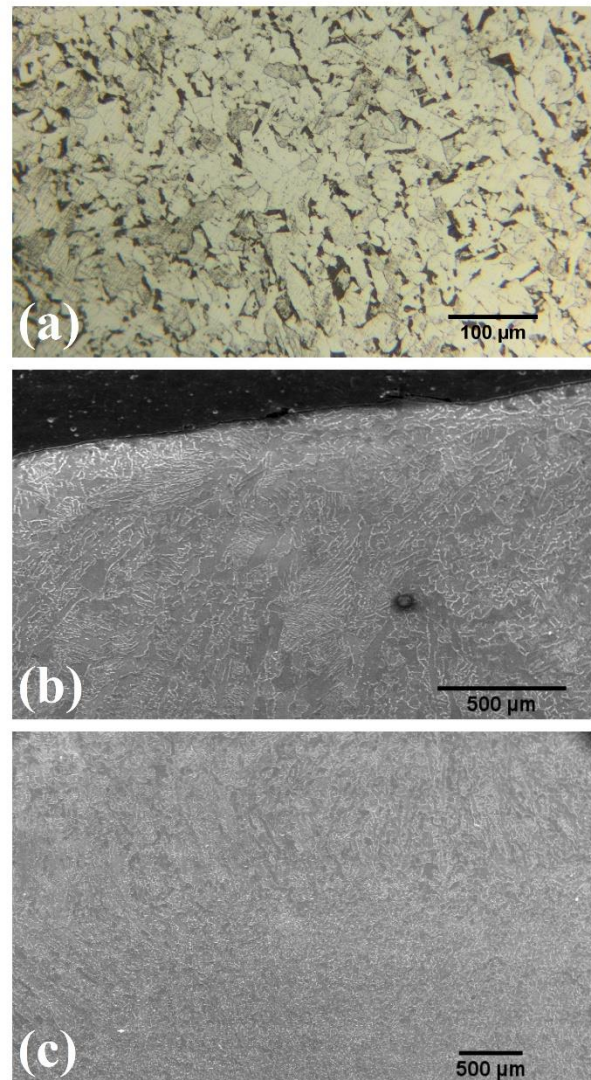


Figure 5. Zone 3 of additive manufacturing steel, evidence of a dendritic structure. (a) Image by optical microscopy, right lateral zone of the last layer, (b) Image by scanning electron microscopy of the left lateral zone of the last layer, (c) Image by scanning electron microscopy of the last layer in the central zone.

3.2. Microhardness

The microhardness results are shown in Figure 6, it is important to remember that each of the layers has an average thickness of the order of $3000 \mu\text{m}$. A behavior that tends to be constant is exhibited, however, there is a slight change in the intermediate zone, this is due to the high homogeneity of the phases, which is linked to the different solidification speeds that make up the material, these results are consistent with those reported by Agredo et al. [8], with a deviation of less than 5% of the reported results. A comparison is established between the layers and the strand, evidencing a greater hardness in the latter, this is related to the severe plastic deformation that the material undergoes in its obtaining process. The steel printing process can be compared to a normalized heat treatment, when it is melted, deposited and slowly cooled to room temperature. In the investigation carried out by Franco and Paz [35], they reveal a hardness after normalized heat treatment of around 130 HV for a material with similar carbon content, in the case of the steel produced in this investigation, a hardness of the order of 150 HV.

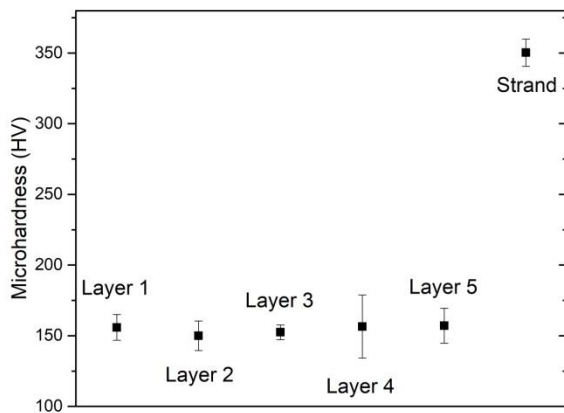
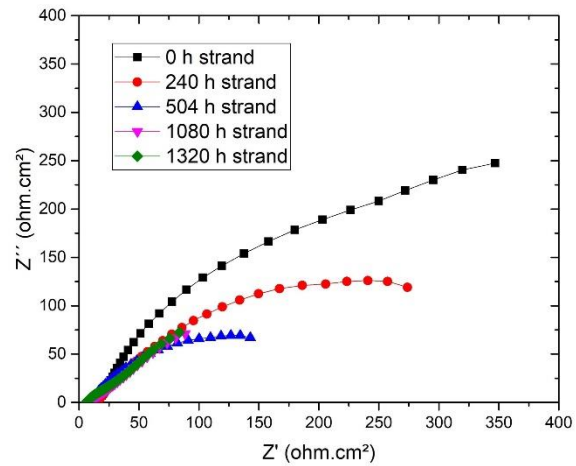


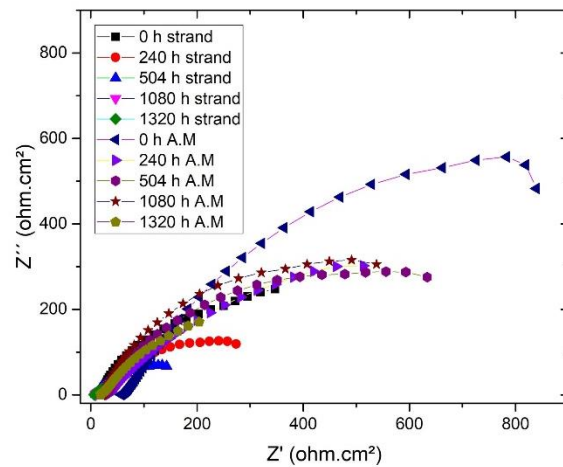
Figure 6. Microhardness of the layers and the filler metal.

3.3. Corrosion monitoring

Figure 7a shows the Nyquist diagram by EIS test for the strand, in Figure 7b, the behavior for the additive manufacturing steel and the strand is observed. In general it is evident the formation of a capacitive-resistive circuit for both materials, there is a clear difference of the printed steel, in this last one is observed an arc of greater diameter, this increase is linked with a greater resistance to the corrosion for the material deposited by layers [36-37]. In both cases the materials show a reduction in the diameter of the arc as the immersion time passes, reflecting a progressive decrease in corrosion resistance.



a)



b)

Figure 7. Nyquist diagram for filament and material by AM.

Figures 8 and 9 show the Bode diagram for the impedance module and the phase angle respectively. The impedance module displays a constant region at high frequencies, this is maintained for the strand and the AM steel, and at low frequencies the sum of the solution resistance and polarization resistance is obtained. However, the impedance experiences a considerable reduction after 1320 h of evaluation, this is due to the degradation of the material with the time of exposure, that is to say, the resistance to polarization decreases. From the phase angle diagram, Figure 9, the strand evidence the formation of only one time constant until 504 hours of evaluation, however, for 1080 and 1320 hours of immersion it is observed the appearance of 2-time constants one located at medium frequencies and another at low frequencies, aspect linked to the appearance of oxides on the surface, depending on the electrochemical behavior seen in the curves, the literature

reports that the formation of oxides on the surface occurs as the appearance of a porous and poorly adherent layer, which does not limit the corrosion process to continue. [38-41,44]. The AM steel, shows the appearance of a single time constant located at medium frequencies for the first hours of evaluation, for 1320 h, a shift towards low frequencies is detailed [13,38,42]. Overall, these results indicate the degradation of the material (AM), due to the electrochemical phenomena that occur in the reaction of the electrolyte and the immersed material, a phenomenon given by the lack of corrosion products that promote a barrier effect on the surface of the material [37,38,43], however, AM steel shows greater resistance to corrosion than the strand.

In AM steel there is a small variation between 504 h and 240 h, achieving a very reduced increase in corrosion resistance, this is due to the formation of a small layer of protective oxides, however, the general behavior of steel is in decay, and the layer of oxides formed does not limit the corrosion process [8], [44].

The average calculation of the corrosion rate for AM steel is made, obtaining a value of 2.34 ± 0.05 mm/year.

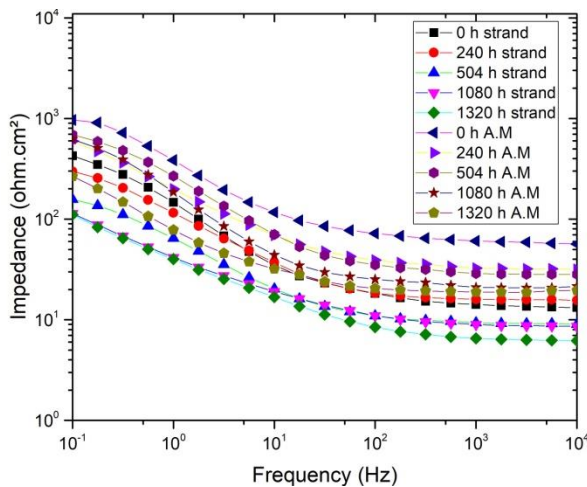


Figure 8. Impedance module for the strand and AM steel.

Moreover, the results acquired by electrochemical noise were analyzed by means of statistical tools. Figure 10 shows the results of the location index calculation for filler metal (strand) and additive manufacturing steel. For the 0 hours of evaluation the filler metal and the additive manufacturing steel present a location index between 0.01 and 0.1, which indicates that mixed corrosion is being presented, after 120 hours of evaluation the strand presents a location index between 0.1 and 1, which identifies that pitting corrosion is occurring, this prevails until 1320 hours of evaluation. In the other hand, the AM

steel at 120 hours of evaluation maintains a mixed corrosion state, already from 504 to 1320 hours this evolves to pitting corrosion [30].

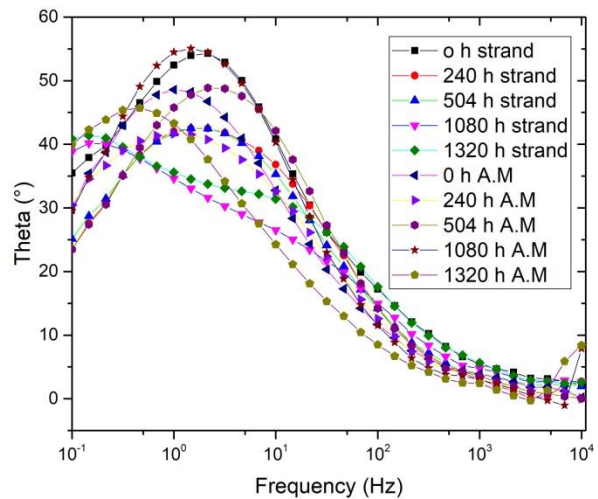


Figure 9. Phase angle for the strand and AM steel.

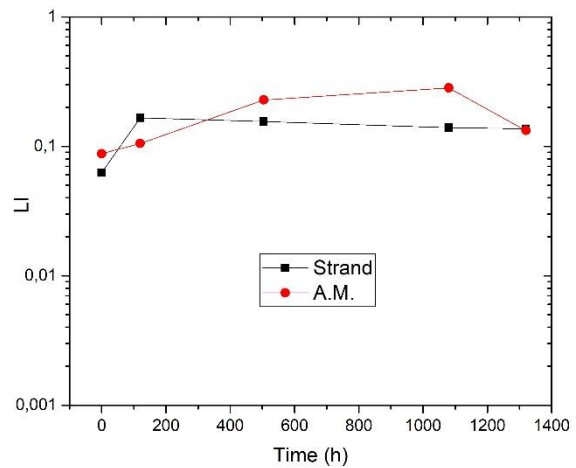


Figure 10. Location index for filler metal and steel by additive manufacture.

The results of the calculation of the noise resistance (R_n) are shown in Figure 11. This parameter is directly related to the corrosion resistance of the materials, this tool has allowed to see that AM steel has a greater resistance to corrosion than the strand, however, again details the degradation of the material, product of the electrochemical phenomena that appear in the system [20,25-26 28]. For 0 hours of immersion both materials show the highest noise resistance value, for the strand, it begins to decline until the end of the test, in the case of AM steel, the noise resistance value drops until 504 h and later evidence a slight increase, this is in accordance with the results presented in EIS.

The stable state of the standard deviation ratio between potential and current density shows that no significant corrosion reactions occur in the samples [26].

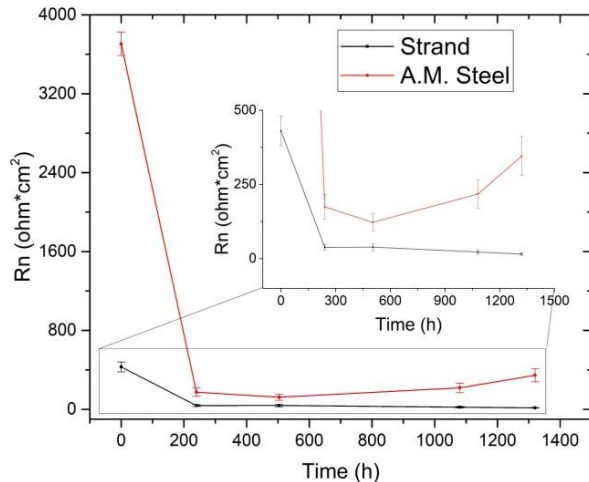


Figure 11. Noise resistance as a function of dive time.

4. Conclusions

The microstructure of the additive manufacturing steel allows the identification of 3 zones, a more homogeneous structure towards the intermediate zone of the steel is evident, with a better distribution of the phases, this translates into a slight increase in the hardness of the material. A dendritic-type microstructure generated by the solidification process is shown for the upper zone of the material.

The corrosion study has determined that the additive manufacturing steel has a greater resistance to corrosion than the strand; however, the nonprotective corrosion products continue to cause the material to degrade as the immersion time passes.

The value of the corrosion rate is calculated from the results in electrochemical noise, obtaining an average value for the additive manufacturing steel of 2.34 mm/year.

The location index shows mixed corrosion for the first hours of evaluation of the 2 materials; however, this is transformed to pitting corrosion from 120 hours of immersion for the strand and from 504 hours for the steel by additive manufacturing, demonstrating that the steel by additive manufacturing presents greater resistance to corrosion.

From the corrosion study, it is considered that it is necessary, for this type of steel produced by the additive

manufacturing technology, to think about coating it to increase its useful life.

Subsequent studies will study the corrosion products generated by the system.

Acknowledgements

The authors would like to thank the PAPIIT IT101318 and PAPIME PE100218 Projects of the DGAPA UNAM for the support for this work.

To the Universidad Nacional de Colombia for the promotion of scientific research and the provision of its facilities, to PhD. Irma Angarita Moncaleano for her collaboration, encouragement and inspiration to work for science.

To the Universidad Pedagógica y Tecnológica de Colombia-UPTC and the research group GSEC, for their collaboration in the development of this project.

References

- [1] A. Hadadzadeh, B. S. Amirkhiz, J. Li, M. Mohammadi, "Microstructure Evolution in Direct Metal Laser Sintered Corrax Maraging Stainless Steel," in *TMS 2019 148th Annual Meeting & Exhibition Supplemental Proceedings*, 2019, pp. 455-462, doi: 10.1007/978-3-030-05861-6_42
- [2] J. J. Cervantes C *et al.*, "Desarrollo de un proceso de manufactura aditiva (AM) de metal y determinación de propiedades de las piezas obtenidas," in *XXIV congreso internacional anual de la SOMIM*, 2018, pp. 20-27.
- [3] V. Thampy *et al.*, "Subsurface Cooling Rates and Microstructural Response during Laser Based Metal Additive Manufacturing," *Sci. Rep.*, vol. 10, no. 1, pp. 1-9, 2020, doi: 10.1038/s41598-020-58598-z
- [4] C. J. Todaro *et al.*, "Grain structure control during metal 3D printing by high-intensity ultrasound," *Nat. Commun.*, vol. 11, no. 1, pp. 1-9, 2020, doi: 10.1038/s41467-019-13874-z
- [5] D. Jia, F. Li, Y. Zhang, "3D-printing process design of lattice compressor impeller based on residual stress and deformation," *Sci. Rep.*, vol. 10, no. 1, pp. 1-11, 2020, doi: 10.1038/s41598-019-57131-1
- [6] B. Zhu, J. Xiong, "Increasing deposition height stability in robotic GTA additive manufacturing based on arc voltage sensing and control," *Robot. Comput. Integr.*

- Manuf.*, vol. 65, pp. 101977, 2020, doi: 10.1016/j.rcim.2020.101977
- [7] T. Duda, L. V. Raghavan, "3D Metal Printing Technology," *IFAC-PapersOnLine*, vol. 49, no. 29, pp. 103-110, 2016, doi: 10.1016/j.ifacol.2016.11.111
- [8] D. G. Agredo-Díaz et al., "Effect of a Ni-P coating on the corrosion resistance of an additive manufacturing carbon steel immersed in a 0.1 M NaCl solution," *Mater. Lett.*, vol. 275, pp. 128-159, 2020, doi: 10.1016/j.matlet.2020.128159
- [9] X. Zhang *et al.*, "Microstructure and mechanical properties of TOP-TIG-wire and arc additive manufactured super duplex stainless steel (ER2594)," *Mater. Sci. Eng. A*, vol. 762, pp. 138097, 2019, doi: 10.1016/j.msea.2019.138097
- [10] Z. Liu *et al.*, "Corrosion and high-temperature tribological behavior of carbon steel claddings by additive manufacturing technology," *Surf. Coatings Technol.*, vol. 384, pp. 125325, 2020, doi: 10.1016/j.surfcoat.2019.125325.
- [11] ASTM, *Electrochemical corrosion testing*. San Francisco: American Society for Testing and Materials, 1979, www.astm.org.
- [12] F. Di Turo, R. Parra, J. Piquero-Cilla, G. Favero, A. Doménech-Carbó, "Crossing VIMP and EIS for studying heterogeneous sets of copper/bronze coins," *J. Solid State Electrochem.*, vol. 23, no. 3, pp. 771-781, 2019, doi: 10.1007/s10008-018-04182-5
- [13] U. P. Morales, Á. M. Camargo, J. J. O. Flórez, "Impedancia electroquímica-interpretación de diagramas típicos con circuitos equivalentes," *DYNA*, vol. 77, no. 164, pp. 69-75, 2010.
- [14] A. Huber *et al.*, "La espectroscopía de impedancia electroquímica (EIS) aplicada al estudio del mecanismo de la corrosión en caliente por sales fundidas," *Dyna*, vol. 71, no. 144, pp. 39-47, 2004.
- [15] R. Cabrera-Sierra, J. Marín-Cruz, I. González, "Comunicaciones técnicas," *Bol. Soc. Quím. Méx.*, vol. 1, no. 1, pp. 32-41, 2007.
- [16] M. Saavedra, "Simulación mediante circuitos equivalentes de la impedancia electroquímica de armaduras de acero inoxidable en mortero," Universidad Carlos III de Madrid, 2014.
- [17] J. Malo-Tamayo, J. Uruchurtu-Chavarín, "La técnica de ruido electroquímico para el estudio de la corrosión," Instituto de Investigaciones Eléctricas. México, 2002.
- [18] S. L. García-Zarco, V. A. Pérez, A. S. García, S. U. Madriñán, Á. S. Bermúdez, "Aplicación de la técnica de ruido electroquímico al estudio de pinturas comerciales de efecto barrera," *Rev. Metal.*, vol. 51, no. 1, pp. 1-8, 2015, doi: 10.3989/revmetalm.039
- [19] J. L. Tristancho, S. Báez, D. Y. Peña, C. Vásquez, "Aplicación de la técnica de ruido electroquímico para la evaluación de la corrosión en caliente por sales fundidas," *Dyna*, vol. 71, no. 144, pp. 85-92, 2004.
- [20] C. A. Loto, "Electrochemical noise measurement technique in corrosion research," *Int. J. Electrochem. Sci.*, vol. 7, no. 10, pp. 9248-9270, 2012.
- [21] D. Escobar, "Estudio de la corrosión mediante la técnica de ruido electroquímico," *Rev ION*, vol. 15, no. 1, pp. 13-23, 1998.
- [22] J. Kearns, D. Eden, M. Yaffe, J. Fahey, D. Reichert, D. Silverman, "ASTM Standardization of Electrochemical Noise Measurement," in *Electrochem. Noise Meas. Corros. Appl.*, 2009, pp. 446-470, doi: 10.1520/stp37976s
- [23] J. Ma, J. Wen, Q. Li, "Electrochemical noise analysis of the corrosion behaviors of Al-Zn-In based alloy in NaCl solution," *Phys. Procedia*, vol. 50, no. October, pp. 421-426, 2013, doi: 10.1016/j.phpro.2013.11.065
- [24] F. Mansfeld, H. Xiao, "Electrochemical Noise and Impedance Analysis of Iron in Chloride Media," in *Electrochem. Noise Meas. Corros. Appl.*, 2009, pp. 59-78, doi: 10.1520/stp37951s
- [25] J. R. Kearns, J. R. Scully, P. R. Roberge, D. L. Reichert, J. L. Dawson, *Electrochemical Noise Measurement for Corrosion Applications*, vol. 100, pp. 19428-2959, 1996, doi: 10.1520/stp1277-eb
- [26] C. A. Loto, "Electrochemical noise measurement and statistical parameters evaluation of stressed α -brass in Mattsson's solution," *Alexandria Eng. J.*, vol. 57, no. 1, pp. 483-490, 2018, doi: 10.1016/j.aej.2016.12.012
- [27] C. A. Loto, R. A. Cottis, "Electrochemical noise generation during stress corrosion cracking of the high-strength aluminum AA 7075-T6 alloy," *Corrosion*, vol. 45, no. 2, pp. 136-141, 1989, doi: 10.5006/1.3577831

- [28] D. Mills, P. Picton, L. Mularczyk, "Developments in the electrochemical noise method (ENM) to make it more practical for assessment of anti-corrosive coatings," *Electrochim. Acta*, vol. 124, pp. 199-205, 2014, doi: 10.1016/j.electacta.2013.09.067
- [29] G199-09, "Standard Guide for Electrochemical Noise Measurement," *ASTM B. Stand.*, vol. 09, pp. 1-9, 2014, doi: 10.1520/G0199-09R14.2
- [30] D. H. Xia, S. Z. Song, Y. Behnamian, "Detection of corrosion degradation using electrochemical noise (EN): review of signal processing methods for identifying corrosion forms," *Corros. Eng. Sci. Technol.*, vol. 51, no. 7, pp. 527-544, 2016, doi: 10.1179/1743278215Y.0000000057
- [31] ASTM International, "ASTM E3.34776 Standard Guide for Preparation of metallographic specimens," *ASTM Stand.*, vol. 11, pp. 1-17, 2017, doi: 10.1520/E0003-11R17.1
- [32] Electrodo Infra, "Ficha técnica: Microalambre sólido infra welding wire 70S-6." *ElectrodoInfra*, pp. 1-2, 2018.
- [33] J. S. Zuback, T. DebRoy, "The hardness of additively manufactured alloys," *Materials (Basel)*, vol. 11, no. 11, 2018, doi: 10.3390/ma11112070
- [34] S. Y. Tarasov, A. V. Filippov, N. N. Shamarin, S. V. Fortuna, G. G. Maier, E. A. Kolubaev, "Microstructural evolution and chemical corrosion of electron beam wire-feed additively manufactured AISI 304 stainless steel," *J. Alloys Compd.*, vol. 803, pp. 364-370, 2019, doi: 10.1016/j.jallcom.2019.06.246
- [35] F. Franco, J. H. Paz, "Tratamiento Térmico de Aceros de Bajo Carbono en Horno de Atmósfera Controlada," *Ing. y Compet.*, vol. 6, no. 2, pp. 56-63, 2004, doi: 10.25100/iyv.v6i2.2278
- [36] H. Saarivirta, P. Rajala, L. Carpen, "Corrosion behaviour of copper under biotic and abiotic conditions in anoxic ground water: electrochemical study," *Electrochim. Acta*, vol. 203, pp. 350-365, 2016, doi: 10.1016/j.electacta.2016.01.098
- [37] B. Wu, Z. Pan, S. Li, D. Cuiuri, D. Ding, H. Li, "The anisotropic corrosion behavior of wire arc additive manufactured Ti-6Al-4V alloy in 3.5% NaCl solution," *Corros. Sci.*, vol. 137, pp. 176-183, 2018, doi: 10.1016/j.corsci.2018.03.047
- [38] J. J. Arenas, M.A., Niklas, A., Conde, A., Méndez, S., Sertucha, J., de Damborenea, "Comportamiento frente a la corrosión de fundiciones con grafito laminar y esférico parcialmente modificadas con silicio en NaCl 0,03 M," *Rev. Metal.*, vol. 50, no. 4, pp. e032, 2014, doi: 10.3989/revmetalm.032
- [39] X. Wen, P. Bai, B. Luo, S. Zheng, C. Chen, "Review of recent progress in the study of corrosion products of steels in a hydrogen sulphide environment," *Corros. Sci.*, vol. 139, no. may, pp. 124-140, 2018, doi: 10.1016/j.corsci.2018.05.002
- [40] L. N. Zhang, O. A. Ojo, "Corrosion behavior of wire arc additive manufactured Inconel 718 superalloy," *J. Alloys Compd.*, vol. 829, pp. 154455, 2020, doi: 10.1016/j.jallcom.2020.154455
- [41] T. Zhang *et al.*, "Corrosion of pure magnesium under thin electrolyte layers," *Electrochim. Acta*, vol. 53, no. 27, pp. 7921-7931, 2008, doi: 10.1016/j.electacta.2008.05.074.
- [42] D. X. Wen, P. Long, J. J. Li, L. Huang, Z. Z. Zheng, "Effects of linear heat input on microstructure and corrosion behavior of an austenitic stainless steel processed by wire arc additive manufacturing," *Vacuum*, vol. 173, no. December, pp. 109-131, 2020. doi: 10.1016/j.vacuum.2019.109131
- [43] I. R. Alvaraz. J. L. Gómez-Pascual, "Caracterización de productos de corrosión del acero al bajo carbono en atmósferas contaminadas por compuestos de azufre," *Ing. y Tecnol.*, vol. IX, pp. 160-170, 2016.
- [44] D. G. Agredo Díaz *et al.*, "Caracterización electroquímica de recubrimientos Zn-Al sobre fundición nodular grado 2, obtenidos por proyección térmica por flama con alambre," *Av. Investig. en Ing.*, vol. 17, no. 1, 2020, doi:10.18041/1794-4953/avances.1.5747